A mixed-valent metal–organic ladder linked by pyrazine

Otake, Ken-ichi; Otsubo, Kazuya; Kitagawa, Hiroshi

IOP Publishing Journal Title
Journal **XX** (XXXX) XXXXXX https://doi.org/XXXX/XXXX

A Mixed-Valent Metal–Organic Ladder Linked by Pyrazine

Ken-ichi Otake[1,2], Kazuya Otsubo[1*] and Hiroshi Kitagawa[1*]

[1] Division of Chemistry, Graduate School of Science, Kyoto University, Kitashirakawa-Oiwakecho, Sakyo-ku, Kyoto 606-8502, Japan
[2] Present address: Institute for Integrated Cell-Material Sciences (iCeMS), Kyoto University, Yoshida, Sakyo-ku, Kyoto 606-8501, Japan
E-mail: kazuya@kuchem.kyoto-u.ac.jp (K. Otsubo), kitagawa@kuchem.kyoto-u.ac.jp (H. Kitagawa)

Received xxxxxx
Accepted for publication xxxxxx
Published xxxxxx

Abstract

We report the synthesis, characterization, and electronic state of a novel mixed-valent metal–organic ladder (MOL) linked by pyrazine (pz). Single-crystal X-ray studies revealed that the MOL has a two-legged ladder-shaped framework, which is composed of a pz-connected Pt dimer with bridging Br ions. The electronic state of the MOL was investigated using X-ray and spectroscopic techniques; the MOL was found to have an electronic state that corresponds to the mixed-valence state of Pt^{II} and Pt^{IV}. Furthermore, the intervalence charge transfer energy of the MOL has lower than that expected from the tendency of a similar halogen-bridged mixed-valence MOL owing to its unique “zig-zag”-shaped legs. These results provide a new insight into the physical and electronic properties of MOL systems.

Keywords: coordination polymer, mixed valency, ladder, platinum complex

1. Introduction

Metal–organic frameworks (MOFs) emerged as a new class of crystalline hybrid inorganic/organic solids, that are composed of metal ions or clusters connected by organic linkers [1–3]. Because of their structural designability and tunable functionalities, MOFs are attracting considerable attention in various applications such as gas storage/separation [4, 5], sensors [6, 7], proton conductors [8, 9], and catalysts [10–12]. More recently, MOFs assembled from electroactive building blocks are being considered appealing for optoelectronic or electrochemical applications [7, 13–15]. However, most MOFs are typically electrical insulators because of the insulating nature of the organic linkers and/or the poor orbital overlap between metal ions through the linkers [15]. To explore the electrical properties of the coordination networks, electron transport pathways must be established through the entire framework. Thus, a judicious choice of organic and inorganic building blocks is requisite. Mixed valency is one of the important factors to be considered for such building blocks because it can endow the framework with interesting electronic and optical properties [16–18]. However, the reports of MOF compounds incorporating mixed-valent moieties are still not common [15].

Among the mixed-valent building bocks, we focus on the one-dimensional (1-D) halogen-bridged mixed-valence transition metal complexes, the so-called MX chains, which has been intensively investigated since the 1970s as a typical example of 1D electron systems [19–22]. The MX-chain compound shows unique chemicophysical properties including luminescence with a large Stokes shift, large third-order nonlinear optical susceptibility, long-range migration of solitons and polarons, and a tunable semiconducting band gap [23–30]. The structure of the MX chain is characterized by an infinite chain, represented as -M–X–M–X–M–X-, composed of metal ions (M = Ni, Pd, Pt) and halide ions (X = Cl, Br, I) (figure 1a). The electronic states of the MX chains can be

categorized into two classifications, depending on the choice of the metal species: Mott–Hubbard (M = Ni^{III}; single valent and paramagnetic) and charge-density-wave (M = $Pd^{II\text{-}IV}$, $Pt^{II\text{-}IV}$; mixed-valent and diamagnetic) states (supplementary figure 1) [19–22]. Recently, to utilize the physicochemical properties derived from the MX chain as the building block, several extended systems of MX chains are reported [31–39]. In these systems, MX chains are linked by organic ligands as rungs and form framework structures with various dimensionalities, namely, metal–organic ladders (MOLs or MX-ladders) [31–35], nanotubes (MONTs or MX-tubes) [36–38], and nanosheets [39] (figure 1b). Interestingly, owing to the interactions among the constituent MX-chains, they show a distinct tendency for its optical band gaps, which differs from that of a single MX chain [32]. This means that the electronic states of the extended MX systems differ from those of the MX chains. Furthermore, with accompanying the increased number of constituent-chains, the ordered valence arrangements were induced among the constituent-chains of the extended MX system [34, 35, 37]. These findings intrigue a wide range of interests in both physicists and chemists in the aspect of the development of the ladder materials, which is typically investigated using oxide-ladder compounds [40–43]. Compared with the conventional oxide-ladder compounds, MOL and MONT compounds based on MX-chains have an advantage in structural designability through the use of coordination chemistry.

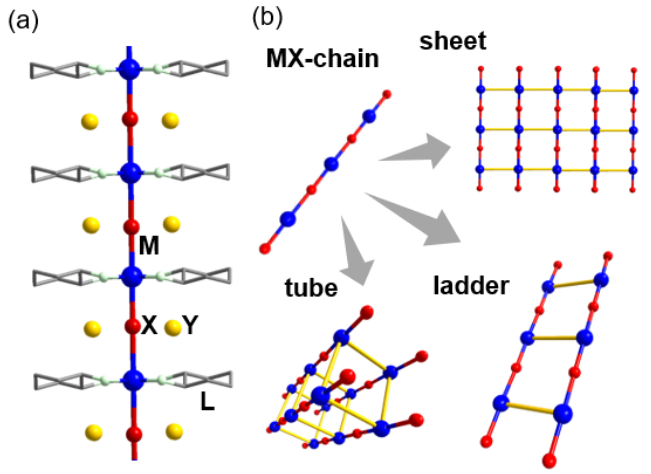

Figure 1. (a) Typical 1-D chain structure of MX-chain compounds. M = Ni, Pd, Pt; X = Cl, Br, I; Y = counter ions; L = capping ligands. (b) Schematic image of the formation of extended MX-systems by connecting chains with rungs

In this work, we describe the synthesis, crystal structure, and electronic state of a novel MOL, [{(dien)PtBr}$_2$(pz)](SO$_4$)$_2$ (**1**) (dien = diethylenetriamine; pz = pyrazine). Two MX chains are connected by pz, forming a two-legged ladder lattice, where the MX chains are the leg. We investigated the electronic state of **1** using X-ray and spectroscopic techniques, which revealed that **1** has an electronic state corresponding to the charge density wave (CDW) state (···Pt^{II}···Br–Pt^{IV}–Br···Pt^{II}···Br–Pt^{IV}–Br··) with the intervalence charge transfer (IVCT) energy of 2.4 eV. The IVCT energy of **1** was lower than that expected from the tendency of IVCT energies of the other MOL systems.

2. Experiment

2.1 Methods

Reagents and solvents were purchased from Wako Pure Chemical Industries, Ltd., TCI Co., Ltd., and Sigma-Aldrich Chemical Co. and were used without further purification.

Elemental Analysis. Elemental analysis was done at the Center for Elementary Analysis (Kyoto University) using a Yanaco MT-5 and MT-6 CHN recorders.

Single Crystal X-ray diffraction analysis (SCXRD). SCXRD data were collected using a Bruker AXS SMART APEX II CCD X-ray diffractometer equipped with the graphite-monochromated Mo-Kα radiation (λ = 0.71073 Å) at 100 K. The structure was solved by a direct method (SIR2004) [44], and refined using full-matrix least squares methods based on F^2 (SHELXL, version 2018/3) [45]. For this analysis, the Yadokari software package [46] was used. The electron densities due to the disordered solvent molecules were squeezed using the PLATON software. Crystallographic data of **1** in the crystallographic information file format have been deposited at the Cambridge Crystallographic Data Centre (CCDC) under deposition number of 2004123. (The data can be downloaded free of charge via www.ccdc.cam.ac.uk/data_request/cif or from Cambridge Crystallographic Data Centre, 12 Union Road, Cambridge CB2 1EZ, U.K.).

Diffuse-reflectance spectroscopy. The diffuse-reflectance spectrum diluted in optical grade calcium fluoride powder was collected using a JASCO V-570 spectrometer equipped with the 60 mm integrating-sphere accessory (ISN-470). Using the Kubelka–Munk function $F(R_\infty)$, the obtained spectrum was transformed into absorption spectra.

Raman spectroscopy. Raman spectra were measured by using a confocal micro-Raman spectrometer (JASCO, NRS-1000). The excitation energy of 532 nm was used (a Showa Optronics model JUNO 532-100S Nd:YAG laser).

X-ray photoelectron spectroscopy (XPS). XPS data were obtained on a SHIMADZU ESCA3400 spectrometer with a monochromatized Mg $K\alpha$ radiation source (1253.6 eV) operated at 6 kV and 10 mA. Samples were ground and spread on a conductive carbon adhesive tape attached to the sample holders. The C 1*s* binding energy of graphite in the carbon tape (284.6 eV) was used to calibrate the binding energy. Curve-fitting analyses were performed using XPS PEAK4.1 software

by using a combination of Gaussian and Lorentzian line shapes.

2.2 Synthesis

[(dien)Pt(NO_3)](NO_3) was synthesized as previously reported [32]. [(dien)Pt(NO_3)](NO_3) (0.10 mmol) and pz (0.05 mmol) were dissolved in water (10 mL), and heated at 80 °C for 1 week. After adding tetramethylammonium hydrogen sulfate (TMA-HSO_4; 0.60 mmol) and then filtering using a membrane filter, the solution was slowly exposed to Br_2 vapour at 5 °C. The film-shapedf shiny-brown crystals of 1 were formed after half a day. The crystals were separated by filtration, washed by a small amount of water, and then dried in air (yield: 30-40%). **Elemental analysis:** Calculated for [{(dien)PtBr}$_2$(pz)](SO_4)$_2$·10H_2O: C, 11.93; H, 4.17; N, 9.27. Found: C, 11.84; H, 3.73; N, 9.18. **Crystal Data:** $C_{12}H_{28}Br_2S_2N_8O_8Pt_2$, M_r = 1026.5, crystal dimensions: 0.30×0.30×0.01 mm^3, monoclinic *C*2/*m*, *a* = 34.20(4) Å, *b* = 5.639(7) Å, *c* = 8.826(11) Å, β =101.33(1) °, *V* = 1669(3) Å^3, *Z* = 2, d_{calcd} = 2.043 g cm^{-3}, μ = 10.933 mm^{-1}, *F*(000) = 956, 1533 unique reflections (out of 6946 with $I > 2\sigma(I)$), Final R_1 ($I > 2\sigma(I)$) = 0.0965, wR_2 (all data)= 0.2480, goodness-of-fit (all data) = 1.172.

3 Results and Discussion

We synthesized the novel ladder compound **1** by a rational bottom-up method using the dinuclear Pt(II) complex [{Pt(dien)}$_2$(pz)](NO_3)$_4$ (dien = 2,2'-diaminodiethylamine; pz

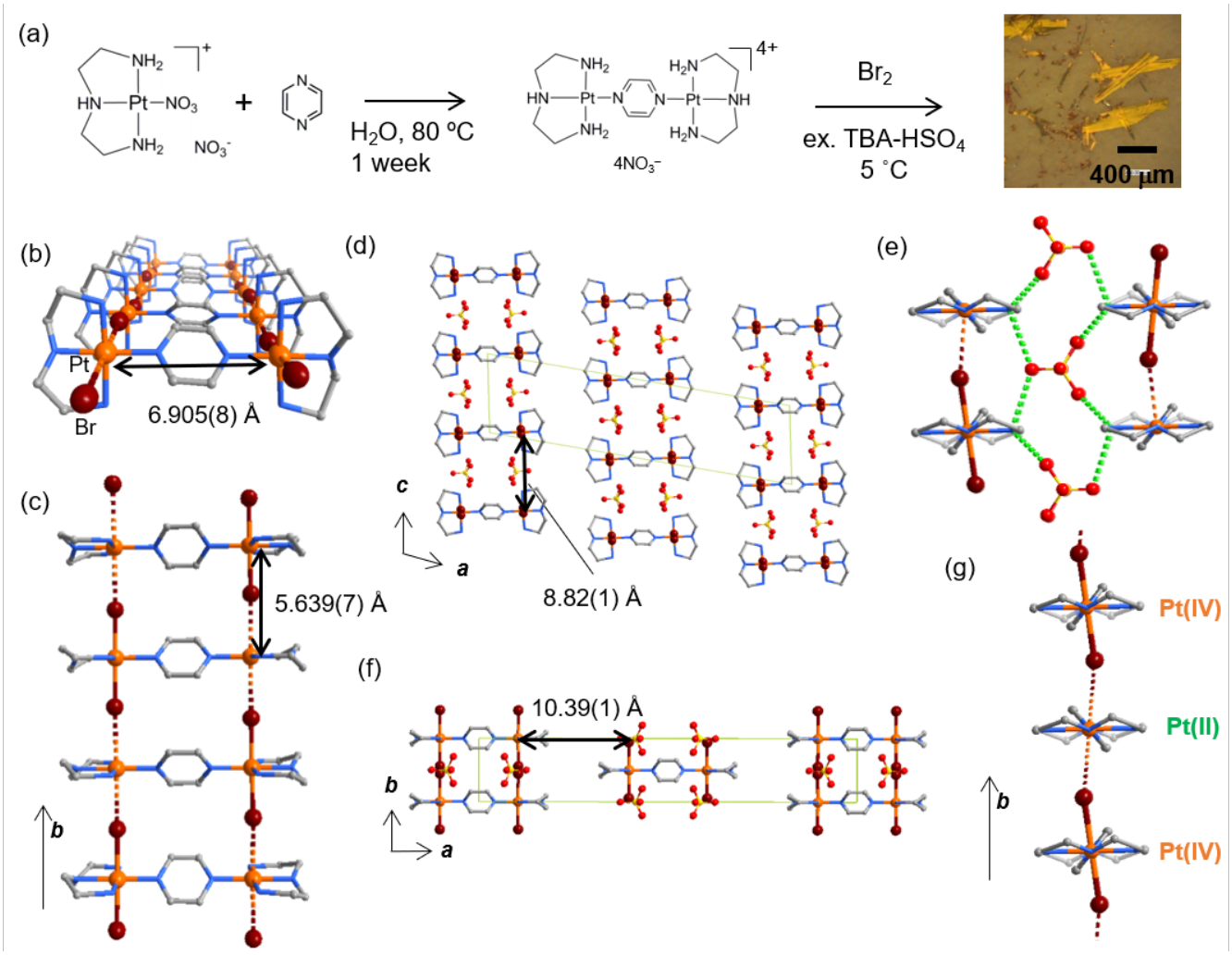

Figure 2. (a) A synthetic scheme of the reporting work and a typical photograph image of single crystals (b-f) Crystal structure (100 K) of **1**. (b) and (c) Two-legged ladder structure. (d) The perspective view of 3D packing in the *ab* plane. (e) Inter-ladder hydrogen bonds between sulfate ion and the ladder lattice of **1** are represented as light-green dotted lines,. The observed distances are between 2.5 and 3.1 Å. (f) Perspective view of 3D packing in *ac* planes. (g) MX leg structure from a side view of the ladder. The spheres represent C (gray), N (blue), O (red), S (yellow), Br (brown) and Pt(orange) atoms, respectively. dien and pz ligands, and bridging Br sites are disordered into two orientations. In panels (b), (c), (e), and (g), one orientation is extracted from the disordered structure for clarity.

= pyrazine) as its building block (figure 2(a)). A partial oxidation reaction [29, 30] using the elemental Br of the divalent Pt precursor afforded the shiny-brown crystals of **1**, [[{PtBr(dien)}$_2$(pz)](SO$_4$)$_2$], as the product of the oxidative polymerization reaction.

The crystal structure of **1** was determined using SCXRD at 100 K (figures 2(b)-(g))). Compound **1** crystallizes in the monoclinic *C2/m* space group with the unit cell parameters of $a = 34.20(4)$ Å, $b = 5.639(7)$ Å, $c = 8.826(11)$ Å, $\beta = 101.33(1)$. As shown in figures 2(b) and 2(c), compound **1** has a clear two-legged ladder structure, where two Br-bridged platinum MX chains constitute its legs. From another viewpoint, pz-connecting dinuclear Pt units were bridged by the Br ion to form an infinite two-legged ladder structure, that propagates along the *b*-axis. In the framework, two chains are separated at 6.905 Å by pz (figure 2(b)), which is the second shortest rung distance among similar halogen-bridged MOLs [31]. In the crystal structure, there are one crystallographically independent Pt site, and two Br sites (Br1A and Br1B in Supplementary figure 2(a)) with quarter occupancies. The bridging Br$^-$ positions deviate from the midpoint between adjacent Pt ions, indicating that the valence state within a constituent chain of **1** corresponds to the mixed-valence state (charge-density-wave state: $\cdots Pt^{II}\cdots Br—Pt^{IV}—Br\cdots$). The Pt-Br distances were determined to be 2.489(3) / 2.506(3) Å and 3.167(4) / 3.184(4) Å, that should correspond to Pt^{IV}—Br and $Pt^{II}\cdots$Br distances, respectively (Supplementary figure 2(b)). Overall, the framework has a net charge of 4+ per [[{PtBr(dien)}$_2$(pz)] unit, which is charge-balanced by two sulfate anions that reside between the ladders as shown in figure 2(d). The ladders are spaced 8.82(1) Å apart in Pt-Pt distances in the *c*-directions, where sulfate anions weakly connect the ladders with hydrogen bonds at the amine group of dien (figure 2(e)). By contrast, the ladders are separated 10.39(1) Å from each other in the *a*-direction (figure 2(f)), where disordered crystallization waters would exist. Interestingly, a unique "zig-zag"-type MX leg is formed in **1** (figure 2(g)) [47, 48]. Such a "zig-zag"-type MX leg has been observed only in once before in {[PtBr(dien)]$_2$(4,4'-bpy)}(NO$_3$)$_4$·2H$_2$O (4,4'-bpy = 4,4'-bipyridine) [34].

To characterize the electronic states of **1**, optical spectra were collected. Raman spectra at room temperature (figure 3(a)) clearly show clear peaks of the symmetrical stretching vibration modes ν(Pt−Br) accompanying the intense overtone at 181 (ν), 362 (2ν), 539 (3ν) cm^{-1}, respectively. In addition, as shown in figure 3(b), an intense and broad peak was observed in the diffuse reflectance spectra at about 2.39 eV, which was assignable to the IVCT from Pt^{II} to the adjacent Pt^{IV} sites. Figure 3c shows the XPS spectra for the Pt 4*f* core-level, which are deconvoluted into two components: one (green color) at the peaks at 72.9 eV (Pt $4f_{7/2}$) and 76.2 eV ($4f_{5/2}$), and the other (orange color) at 74.8 eV (Pt $4f_{7/2}$) and 78.0 eV ($4f_{5/2}$). These pairs of peaks can be attributable to the Pt^{2+} and Pt^{4+} components in the compound, respectively. These spectroscopic results clearly demonstrate that the electronic state of **1** is the CDW state ($\cdots Pt^{2+}\cdots Br—Pt^{4+}—Br\cdots$) and correspond to the class II compounds of the Robin–Day classification [49], consistent with the SCXRD result.

In the MX-chain compounds, the distortion parameter (*d*) is a good parameter that well-represents its electronic state [34, 35, 50, 51]. The *d* parameter is expressed as $d = (l_1 - l_2)/L_0$, that is calculated from Pt−Pt distance (L_0) and the Pt−X distances (l_1 for $Pt^{2+}\cdots X$; l_2 for $Pt^{4+}—X$). Figure 4a shows the plots of L_0 against l_1 or l_2 for several MX-chain (shown as black marker) and MOL compounds (shown as blue markers). As clearly seen, there is a linear relationship among L_0, l_1 and l_2 distances, which is highly dependent on the bridging halide (circles for chloride-, triangles for bromide-, and square for

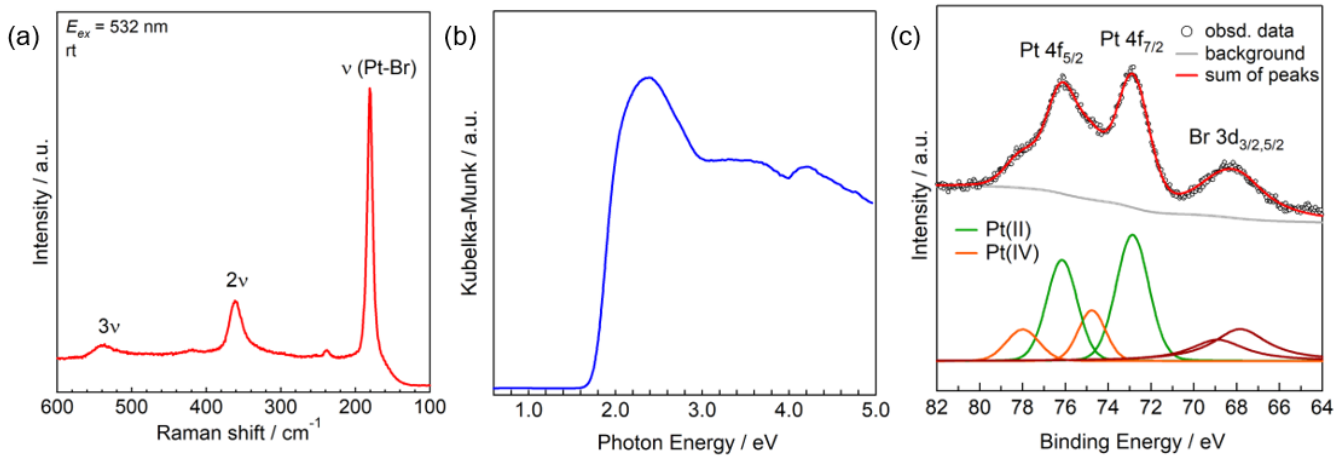

Figure 3. (a) Raman spectrum at room temperature (the excitation energy of 532 nm). The intense peaks of the symmetrical stretching modes ν(Pt-Br) with overtones were clearly observed at 181 cm^{-1}. (b) Diffuse reflectance spectrum at room temperature, (c) XPS spectra and fitting results. Pt $4f_{7/2}$ and $4f_{5/2}$ core-level spectra are shown. Br 3*d* core-level spectra were also observed at the similar binding energy at 68.2 eV.

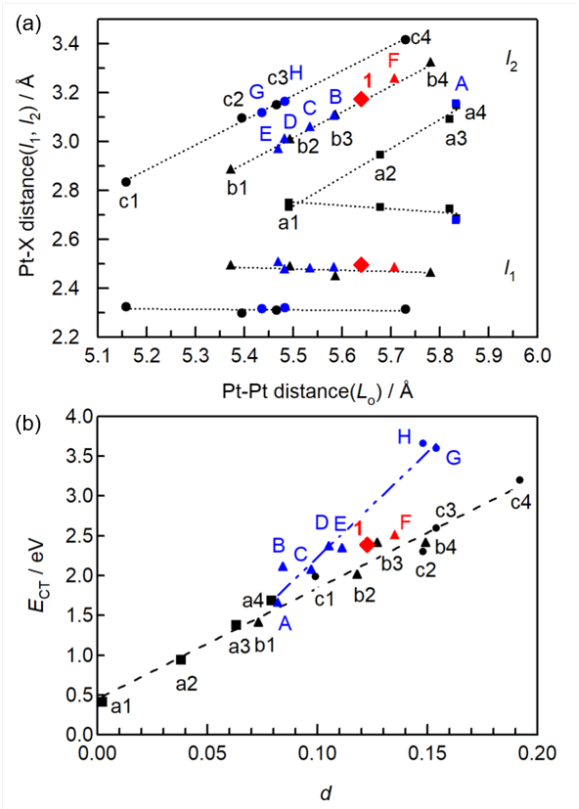

Figure 4. (a) Plots of the Pt–Pt (L_0) against Pt–X (l_1 and l_2) distances of MX compounds. The dotted lines are least-square fits of l_1 and l_2 depending on the briding-halogen species. (b) Plots of E_{CT} against the d parameter. The dotted lines are least-square fits of E_{CT} of MX-chain (black line) and two-legged MOL (excepting 1 and F; blue line) systems. Circle, triangle, and square symbols denote the chloride-, bromide-, and iodide-bridged MX compounds, respectively. Black and blue symbols represent the data for the MX-chain and two-legged MOL systems, respectively. The zig-zag-typed two-legged MOL is represented as red triangle marker. The data of the compound **1** is shown as red diamond marker. In these plots, data are shown for MX chain (a1~c4): (a1) $[PtI(en)_2](L\text{-Asp-}C_{10})_2\cdot H_2O$, (a2) $[PtI(chxn)_2]I_2$, (a3) $[PtI(en)_2](ClO_4)_2$, (a4) $[PtI(NH_3)_4](HSO_3)_3(OH)$, (b1) $[PtBr(chxn)_2]Br_2$, (b2) $[PtBr(etn)_2]Br_2$, (b3) $[PtBr(en)_2](ClO_4)_2$, (b4) $[PtBr(chxn)_2](ClO_4)_2$, (c1) $[PtCl(chxn)_2]Cl_2$, (c2) $[PtCl(tn)_2](BF_4)_2$, (c3) $[PtCl(NH_3)_4](HSO_3)_4$, (c4) $[PtCl(chxn)_2](ClO_4)_2$; MOL (A~H): (A) $[\{PtI(en)\}_2(2,2'\text{-bpym})]I_4\cdot 4H_2O$, (B) $[\{PtBr(dien)\}_2(4,4'\text{-bpy})]Br_4\cdot 2H_2O$, (C) $[\{PtBr(en)\}_2(2,2'\text{-bpym})]Br_4\cdot 4H_2O$, (D) $[\{PtBr(en)\}_2(2,2'\text{-bpym})]Br(ClO_4)_3\cdot H_2O$, (E) $[\{PtBr(dien)\}_2(4,4'\text{-chxn})](NO_3)_4$, (F) $[\{PtBr(dien)\}_2(4,4'\text{-bpy})](NO_3)_4$, (G) $[\{PtCl(en)\}_2(2,2'\text{-bpym})]Cl\text{-}(ClO_4)_3\cdot H_2O$, (H) $[\{PtCl(chxn)\}_2(4,4'\text{-azpy})](ClO_4)_4\cdot C_3H_6O$.

iodide-bridged MX compounds in figure 4) [50, 51]. In general, a shorter L_0 induces the orbital overlap between platinum $5d_z^2$ and halide p_z orbitals, thus resulting in shorter l_2 and longer l_1 distances. These parameters of MOL compounds also fell on the same lines as those of the MX chains (the blue symbols in figure 4(a)); Compound **1**, shown as a red diamond, also falls on the same line. Figure 4(b) displays the correlation between d and the IVCT energies (E_{CT}). Linear relationships were observed for both the MX-chain and MOL compounds. However, by contrast with the results seen in figure 4a, their tendencies differ from each other; the slope of the MOL is higher than that of the single MX-chain system. According to the extended Peierls–Hubbard model, the E_{CT} of an MX chain can be expressed as $E_{CT} = 8S - U + 3V$, where the physical parameters represent the electron–lattice interaction (S) and the onsite (U) and intersite (V) Coulomb repulsions along the MX chain (supplementary figure 3). [52–55] For the two-legged MOL, the E_{CT} can be described as $E_{CT} = 8S - U + 3V + 2V'$, where V' is either the through-rung (V_{rung}) or diagonal (V_{diag}) Coulomb interaction within the ladder (supplementary figure 3) [34, 35, 52–55]. By contrast, the tendency of E_{CT} of **1** deviates from the other MOL systems. This can be explained by the "zig-zag"-shaped MX legs of **1** as similar to another zig-zag-shaped MOL (entry F in figure (b)) [34]; the interchain Coulomb repulsion along the chain (V) would be reduced by the "zig-zag"-shaped MX-leg as shown in figure 2(f).

4. Conclusions

In conclusion, we have successfully fabricated a novel MOL compound with pz as the bridging ligand. Single-crystal X-ray studies showed that the legs of the ladder is composed of MX-chains. We investigated the electronic state of $[\{(dien)PtBr\}_2(pz)](SO_4)_2\cdot 10H_2O$ using X-ray and spectroscopic techniques, and found that the electronic state corresponds to the CDW state. Furthermore, from the tendency of IVCT energies of the other metal–organic ladder systems, we found the IVCT energy of 1 to be lower than the expected, probably because of the "zig-zag"-shaped MX-legs that weaken the interchain Coulomb repulsion. We believe that incorporating a mixed-valent moiety into the framework of the coordination polymer would open up the elusive electronic functionalities in the MOF chemistry. Our exploration of the MX-chain-based multi-dimensional frameworks having various functionalities and electronic properties is in progress [34–39].

Acknowledgements

This work was supported by Core Research for Evolutional Science and Technology (CREST) "Creation of Innovative Functions of Intelligent Materials on the Basis of the Element Strategy", ACCEL from Japan Science and Technology

Agency (JST), JSPS KAKENHI Grant Numbers JP20350030, JP23245012, JP15H05479, JP17H05366, JP19K05494 and JP19H04572 (Coordination Asymmetry).

ORCID iDs

Ken-ichi Otake: https://orcid.org/0000-0002-7904-5003
Kazuya Otsubo: https://orcid.org/ 0000-0003-4688-2822
Hiroshi Kitagawa: https://orcid.org/ 0000-0001-6955-3015

References

[1] Kitagawa S, Kitaura R, Matsuzaka H, Noro S 2004, *Angew. Chem. Int. Ed.* **43** 2334
[2] Ferey G 2008 *Chem. Soc. Rev.* **37** 191
[3] Furukawa H, Cordova K E, O'Keeffe M, Yaghi O M 2013 *Science* **341** 1230444
[4] Ma S and Zhou H 2009 *Chem. Commun.* **46** 44
[5] Horike S, Shimomura S, Kitagawa S 2009 *Nature Chemistry* **1** 695
[6] Stavia V, Talin A A, Allendorf M D 2014 *Chem. Soc. Rev.* **43** 5994
[7] Shekhah O, Liu J, Fischer R A, Wöll Ch 2011 *Chem. Soc. Rev.* **40** 1081
[8] Sadakiyo M, Yamada T, Kitagawa H 2009 *J. Am. Chem. Soc.* **131** 9906
[9] Ramaswamy Padmini, Wong N E, Shimizu G KH 2014 *Chem. Soc. Rev.* **43** 5913
[10] Lee J, Farha O K, Roberts J, Scheidt K A, Nguyen S T, Hupp J T 2009 *Chem. Soc. Rev.* **38** 1450
[11] Liu J, Chen L, Cui H, Zhang J, Zhang L, Su C-Y 2014 *Chem. Soc. Rev.* **43** 6011
[12] Otake K, Cui Y, Buru C T, Li Z, Hupp J T, Farha J T 2018 *J. Am. Soc. Chem.* **140** 8652
[13] Morozan A and Jaouen F 2012 *Energy Environ. Sci.* **5** 9629
[14] Stassen I, Burtch N, Talin A, Falcaro P, Allendorf M, Ameloot R 2017 *Chem. Soc. Rev.* **46** 3185
[15] Xie L S, Skorupskii G, Dincã M 2020 *Chem. Rev.* doi:10.1021/acs.chemrev.9b00766
[16] Robin M B, Day P 1967 *Adv. Inorg. Chem. Radiochem.* **9** 247
[17] Tokura Y, Taguchi Y, Okada Y, Fujishima Y, Arima Y, Kumagai K, Iye Y 1993 *Phys. Rev. Lett.* **70** 2126
[18] Murase R, Leong C F, D'Alessandro D M 2017 *Inorg. Chem.* **56** 14373
[19] Kida S 1965 *Bull. Chem. Soc. Jpn.* **38** 1804
[20] Interrante L V, Browall K W, Bund F P 1974 *Inorg. Chem.* 1**3** 1158
[21] Clark R J H, Kurmoo M, Galas A M R, Hurshouse M B 1983 *J. Chem. Soc., Dalton Trans.* **1983** 1583
[22] Okamoto H and Yamashita M 1992 *Phys. Rev. Lett.* **69** 2248
[23] Takaishi S, Miyasaka H, Sugiura K, Yamashita M, Matsuzaki H, Kishida H, Takami T 2004 *Angew. Chem. Int. Ed.* **43** 3171
[24] Takaishi S, Takamura M, Kajiwara T, Miyasaka H, Yamashita M, Iwata M, Matsuzaki H, Okamoto H, Tanaka H, Kuroda S, Nishikawa H, Oshio H, Kato K, Takata M 2008 *J. Am. Chem. Soc.* **130** 12080
[25] Kishida H, Matsuzaki H, Okamoto H, Manabe T, Yamashita M, Taguchi Y, Tokura Y 2000 *Nature* **405** 929
[26] Kimura K, Matsuzaki H, Takaishi S, Yamashita M, Okamoto H 2009 *Phys. Rev. B: Condens. Matter Mater. Phys.* **79** 075116
[27] Kimura K, Matsuzaki H, Takaishi S, Yamashita M, Okamoto H. 2009 *Phys. Rev. B* **79** 075116
[28] Iguchi H, Takaishi S, Jiang D, Xie J, Yamashita M, Uchida A, Kawaji H 2013 *Inorg. Chem.* **52** 13812
[29] Otake K, Otsubo K, Sugimoto K, Fujiwara A, Kitagawa H 2016, *Inorg. Chem.* **55**, 2620
[30] Mian M R, Iguchi H, Takaishi S, Murasugi H, Miyamoto T, Okamoto H, Tanaka H, Kuroda S-i, Breedlove B K and Yamashita M 2017 *J. Am. Chem. Soc.* **139** 6562
[31] Kawakami D, Yamashita M, Matsunaga S, Takaishi S, Kajiwara T, Miyasaka H, Sugiura K, Matsuzaki H, Okamoto H, Wakabayashi Y, Sawa H 2006 *Angew. Chem. Int. Ed.* **45** 7214
[32] Kobayashi A and Kitagawa H 2006 *J. Am. Chem. Soc.* **45** 7214
[33] Yamada T, Otsubo K, Makiura R, Kitagawa H 2013 *Chem. Soc. Rev.* **42** 6655
[34] Otsubo K, Kobayashi A, Sugimoto K, Fujiwara A, Kitagawa H 2014 *Inorg. Chem.* **53** 1229
[35] Otsubo K and Kitagawa H 2014 *CrystEngComm* **16** 6277
[36] Otsubo K, Wakabayashi Y, Ohara J, Yamamoto S, Matsuzaki H, Okamoto H, Nitta K, Uruga T, Kitagawa H 2011 *Nat. Mater.* **10** 291
[37] Otake K, Otsubo K, Sugimoto K, Fujiwara A, Kitagawa H 2016 *Angew. Chem. Int. Ed.* **55** 6448
[38] Otake K, Otsubo K, Komatsu T, Dekura S, Taylor J M, Ikeda R, Sugimoto K, Fujiwara A, Chou C-P, Sakti A W, Nishimura y, Nakai H, Kitagawa H 2020 *Nat. Commun.* **11** 843
[39] Hashiguchi R, Otsubo K, Maesato M, Sugimoto K, Fujiwara A, Kitagawa H 2017 *Angew. Chem. Int. Ed* **56** 3838
[40] Azuma M, Hiroi Z, Takano M, Ishida K, Kitaoka Y 1994 *Phys. Rev. Lett.* **73** 3463
[41] Hiroi Z and Takano M 1995 *Nature* **377** 41
[42] Blumberg G, Littlewood P, Gozar A, Dennis B S, Motoyama N, Eisaki H, Uchida S 2002 *Science* **297** 584
[43] Abbamonte P, Blumberg G, Rusydi A, Gozar A, Evans P G, Siegrist T, Venema L, Eisaki H, Isaacs E D, Sawatzky G A 2004 *Nature* **431** 1078
[44] Burla M C, Caliandro R, Camalli M, Carrozzini B, Cascarano G L, De Caro L, Giacovazzo C, Polidori G and Spagna R 2005 *Journal of Appl. Cryst.* **38** 38
[45] Sheldrick G 2015 *Act. Cryst. Sec. C* **71** 3
[46] Kabuto C, Akine S, Nemoto T, Kwon E 2009 *J. Cryst. Soc. Jpn.* **51** 218
[47] Clark R J H, Kurmoo M, Galas A M R, Murstouse M B 1983 *J. Chem. Phys. Datlon. Trans.* **1983** 1583
[48] Mian M R, Afrin U, Iguchi H, Takaishi S, Yoshida T, Miyamoto T, Okamoto H, Tanaka H, Kuroda S, Yamashita M 2020 *CrystEngComm* (Advanced Article)
[49] Robin M B, Day Peter 1968 *Adv. Inorg. Chem. and Radiochem.* **10**, 247.
[50] Okamoto H, Mitani T, Toriumi K, Yamashita M 1992 *Mater. Sci. Eng., B* **13** L9.

[51] Scott B, Love S P, Kanner G S, Johnson S R, Wilkerson M P, Berkey M, Swanson B I, Saxena A, Huang X Z, Bishop A R 1995 *J. Mol. Struct.* **356** 207
[52] Funase K and Yamamoto S 2006 *J. Phys. Soc. Jpn.* **75** 044717.
[53] Yamamoto S and Ohara J 2007 *J. Phys. Rev. B: Condens. Matter Mater. Phys.* **76** 235116
[54] Iwano K and Shimoi Y 2007 *J. Phys. Soc. Jpn.* **76** 063708.
[55] Yamamoto S and Ohara J 2009 *J. Mater. Sci.: Mater. Electron.* **20** 367.